Journal of Materials Chemistry C

Accepted Manuscript

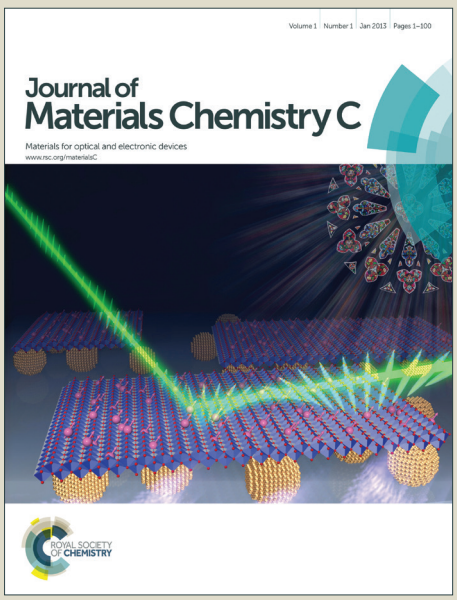

ROYAL SOCIETY OF CHEMISTRY

www.rsc.org/materialsC

Journal of Material Chemistry C

ARTICLE

Tailored sunlight driven nano-photocatalyst: Bismuth iron tungstate ($BiFeWO_6$)

Received 00th January 20xx,
Accepted 00th January 20xx

DOI: 10.1039/x0xx00000x

www.rsc.org/

R. Radha,[a] A. Srinivasan[a] P. Manimuthu[b] and S. Balakumar[a,*]

The challenge in employing tungstates for photocatalytic water splitting is to position their conduction bandoffset with that of the redox potential. As envisaged in Bi_2WO_6, conduction band minimum (CBM) is shifted but the bandgap energy value is around 3.1 eV. Thus the strategy of shifting the CBM and reducing the band gap energy is demonstrated to tailor a novel sunlight driven visible light photocatalyst. Accordingly, $BiFeWO_6$ nanoparticles (BFWO NPs) have been synthesized by a facile co-precipitation method. The X-Ray diffraction results confirmed that the structure of BFWO is a defect pyrochlore. The FESEM images revealed spherical morphology, and the particle size range 15nm to 30nm was observed from HRTEM images. The optical band gap energy of the synthesized BFWO NPs was estimated to be 2.35eV using the UV-DRS spectrum and CBM is positioned with respect to its electronegativity. The photocatalytic activity of the synthesized BFWO NPs was investigated on the degradation of methylene blue under direct irradiation of sunlight and the observed efficiency is explained with the crystal field theory.

Introduction

"Energy Needs Water and Water Needs Energy" stated by UNWWAP (United Nation World Water Assessment Programme) in 2014, undoubtedly demonstrates the utilization of water as resource for the fuel productions and necessity of clean water. Towards achieving this, semiconductor photocatalysis is green technology to photolyse water for hydrogen generation and for photoremediation of contaminated water.[1-3] Intense research in this field, particularly over the last two decades, has led to the discovery of several new classes of materials as well as several strategies with which material's photocatalytic property can be tuned by inducing physical and chemical modifications. These explorations have helped to develop novel materials and understand their photocatalytic phenomena.

For instance, the conventional photocatalysts, such as TiO_2, ZnO, CdSe, have poor visible light utilisation, and stability issues.[4-5] Addressing these issues would need effective strategies such as chemical substitution, doping, compositing.[6-8] However such modification in turn increases the complexity of the photocatalysts in terms of their chemical composition. Hence, identifying a stable, single phase material is a topic of interest in the photocatalytic research. Apart from optimal band gap as a prerequisite, an efficient photocatalyst should also hold good crystalline nature with controlled particle size to facilitate the effective separation and migration of the photogenerated carriers in the photocatalyst.[9]

In pursuit of such materials, pyrochlore structured material offers band gap in the visible region and a manipulative crystal structure that can be desired to develop an ideal photocatalyst.[10] The general chemical formula of pyrochlores is $A_2B_2O_7$, of which AB_2O_6 is a β-pyrochlore which is a defective structure. These β-pyrochore structured materials, in particular grab attention, as they offer the ability to manipulate electron/hole mobility by the choice of different elements introduced in different sites.[11] Also, the combinational variations made in 'A', 'B', and oxygen sites and in structural parameters such as bond length, bond angle together contribute in the electronic structure influencing the photocatalytic behaviour.[12-13]

Among such β-pyrochlore materials, bismuth (Bi) based pyrochlores are known for visible light driven photocatalytic activity owing to the hybridization of Bi 6s – O 2p orbitals. Such band gap engineering in other Bi based photocatalytic materials has been widely reported in literature that broadly include ferrites ($BiFeO_3$)[14], titanate ($Bi_2Ti_2O_7$)[15], tungstate (Bi2WO6)[16], vanadate (BiVO4)[17], niobate (Bi_2FeNbO_7)[18]. For instance, it is reported that the incorporation of Bi in the TiO_2 lattices leads to the formation of $Bi_2Ti_2O_7$ pyrochlore structure that exhibited band gap energy of 2.6 eV while the band gap energy of typical TiO_2 is 3.2 eV.[19] Valent et al. has reported the lowest band gap energy of 1.96 eV among the Bi based pyrochlore compounds (Bi-Fe-Te-O).[20]

On the other hand, WO_3 has band gap of 2.6 – 3.1 eV which is lower than TiO_2, enables it to be driven by longer wavelengths.[21] However, as the conduction band minimum (CBM) is being more positive than the standard hydrogen

[a,a*] National Centre for Nanoscience and Nanotechnology, University of Madras, Maraimalai Campus, Chennai 600 025, India. Fax: 044-22352494/ 22353309; Te: 044-22202749, *E-mail: balasuga@yahoo.com
[b,b] Department of Nuclear Physics, University of Madras, Maraimalai Campus, Chennai 600 025, India.
Electronic Supplementary Information (ESI) available

potential (+0.5 V vs. NHE), no spontaneous hydrogen generation and overall water splitting can be achieved in pure WO_3.[22] To tune the electronic structure, WO_3 can be fused with other metal oxides to form binary and ternary tungstates.[23] Among such bismuth based tungstates, Bi_2WO_6 is a known photocatalyst that has a band gap energy of 2.8 - 3.1 eV which has been used for water splitting application.[24]

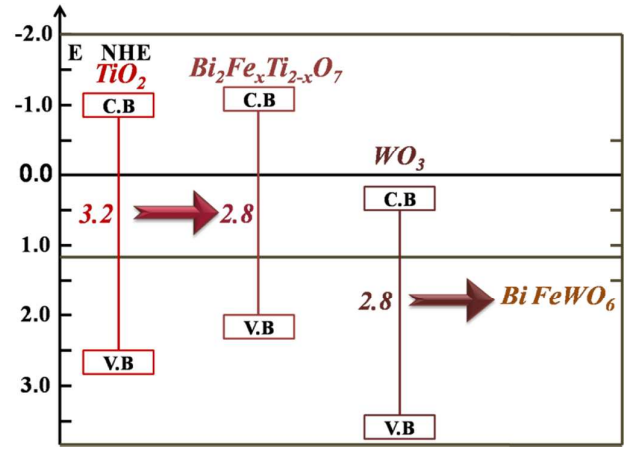

Figure. 1. Schematic comparison of the band gap energy and bandedge offset for titanate and bismuth iron titanate and hence for the tungstate.

Fig.1 schematically shows the comparison of the band gap for titanate and bismuth iron titanate and hence the concept to study Bismuth iron tungstate pyrochlore. Ramanan et al. has reported the stabilisation of pyrochlore bismuth iron tungstate over perovskite on inclusion of 3*d* transition elements.[25] Based on these studies keen interest provoked to analyse the optical properties of pyrochlore structured $BiFeWO_6$.

Recently $BiFeWO_6$ of monoclinic phase was studied by Rout et al. for its electrical property.[26] To the best of our knowledge this is the first report on the optical property of $BiFeWO_6$ nanoparticles for its application in photocatalytic degradation of organic pollutants under direct irradiation of sunlight. Accordingly, this work is intended to synthesize the nanoparticles of $BiFeWO_6$ by a facile co-precipitation method and to characterize their thermal, structural, morphological, optical, and photocatalytic properties.

Materials and Methods

Chemicals

All the chemicals used for the study were of analytical grade with high purity (99.9%), procured from commercial resource (Alfa Aesar).

Preparation of photocatalyst

$BiFeWO_6$ nanoparticles were synthesized by a facile co-precipitation method. In the typical synthesis process, an equal molar ratio of $Bi(NO_3)_3{\cdot}5H_2O$, $Fe(NO_3)_3{\cdot}9H_2O$, and Na_2WO_4 $2H_2O$ were homogenously dissolved in double distilled water. To this, an equal concentration of ammonia (NH_4OH) solution was slowly dripped and obtained the precipitation. Then the precipitate was collected and washed with double distilled water and ethanol for several times and dried at 100 ^{0}C for 3 h. Subsequently the end product was annealed at 600 ^{0}C for 6 h to obtain the phase of the material.

The above said experimental conditions were followed to prepare Bi_2WO_6 (BW) particles, which is used as standard reference to compare the optical property of the BFW NPs.

Photocatalytic activity

Before extending to water splitting application, the photocatalytic efficiency of $BiFeWO_6$ was delved over the degradation of the heteropolyaromatic dye-methylene blue (MB). In a typical experiment, 10mg of MB dye was dissolved in 1000ml of water, of which 100ml was isolated and tested for degradation. 100 mg of BFWO NPs was dispersed in 100 ml of MB solution. Before exposure, the suspensions were stirred in dark for 30 minutes to ensure the establishment of adsorption/desorption equilibrium of MB on the sample surfaces. The suspension were then exposed to direct sunlight during the sunny days of April 2014 in Chennai city between 11.00 a.m. – 3.00 p.m., the then observed intensity using a luxmeter was 120000 lux. Consequently 5 ml of suspension at regular time interval were centrifuged at a rate of 6000 rpm for 10 minutes. The same procedure was repeated for commercially available TiO_2 and the prepared Bi_2WO_6 to obtain the standard photocatalytic efficiency. Photodegradation of MB dye, which has characteristic absorption peak at 664 nm was monitored by UV-vis absorption spectra obtained by using Perkin Elmer Lambda 650s spectrophotometer. The rate of mineralisation of MB was also monitored using total organic carbon (TOC) analyser (Shimadzu TOC- L instrument, Japan). Under similar experimental procedure BFWO NPs photocatalytic degradation efficiency was tested against 50 ppm of colourless phenol using 300 W tungsten lamp as light source.

The formation of OH radicals by BFWO NPs was analysed using terephthalic acid as probe. 50 ml of 3mmol of terephthalic acid and 2mmol of NaOH solution were used to disperse 50 mg of BFWO NPs. The suspension was stirred in dark for 60 minutes before irradiation of visible light (300 W tungsten lamp). Then 4 ml of solution were pipetted out and centrifuged at 60 minutes time interval. The supernatant was examined for fluorescence using Perkin Elmer LS45 luminescence spectrophotometer. The photogenerated OH radicals react with terephthalic acid to form 2-hydroxyterephthalic acid (TAOH), which was excited at 312nm and observed a fluorescence band at 426 nm. The increase in fluorescence intensity is directly proportional to the generated OH radicals.

The electrochemical impedance spectroscopy (EIS) measurments were performed in the presence of 5.0 mM $K_3[Fe(CN)_6]/K_4[Fe(CN)_6]$ by applying an AC voltage with 5 mV amplitude in a frequency range from 1 Hz to 85 kHz under open circuit potential conditions.

Results and discussion

Thermal Analysis

The thermal decomposition of the as-prepared product was analyzed using thermo gravimetric analysis (TGA, TG/DTA 6300) and the result is shown in Fig. 2. From the curve, it is clearly seen a weight loss in the region 70 ^{0}C – 200 ^{0}C and 200 ^{0}C – 300 ^{0}C. This corresponds to the vapourisation of the adsorbed water molecules, nitrates and ammonia compounds. A plateau region observed up to 520 ^{0}C indicates that no more volatile substances are to be evaporated. Such observation is also reflected in the DTA curve, where the peak observed at 520 ^{0}C could be due to the transition from amorphous to crystalline phase.

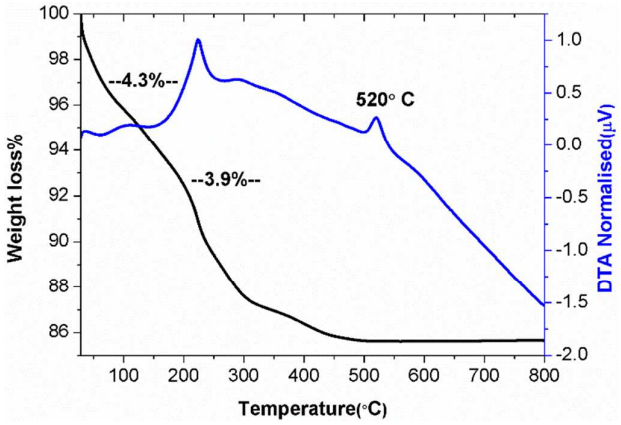

Figure. 2 TG and DTA curve of BiFeWO6

Structural Analysis

X-ray diffraction analysis was performed using Cu-Kα radiation (λ= 1.541838 Å) with 2θ in the range 20º to 70º and a step size of 0.02 (RIGAKU X ray diffractometer).Fig 3 shows the X ray diffraction pattern of the prepared BFWO NPs.

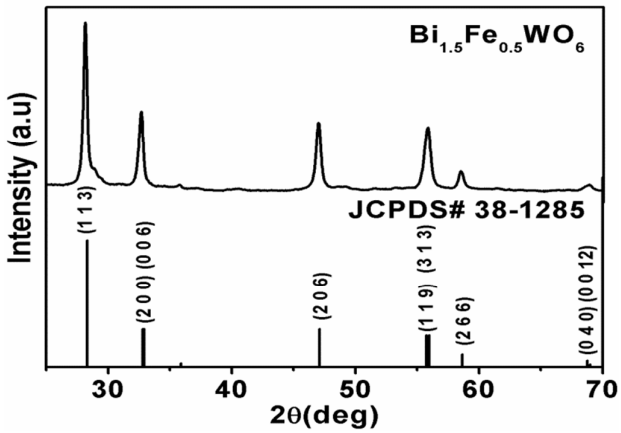

Figure. 3 Powder X- ray diffraction pattern of $BiFeWO_6$

XRD result depicts that the prepared sample is highly crystalline and is in good agreement with the standard diffraction pattern (JCPDS #38-1285). The XRD peaks are well indexed to the orthorhombic structure with the lattice parameters a = 5.582 Å, b = 5.524 Å, c = 16.064 Å, and cell volume (V) = 495.31 Å^3. Similarly, the crystallite size was calculated using Scherrer's formula corresponding to the (113) plane and is found to be 30 nm. The XRD pattern also evidences that the obtained BiFeWO6 has no secondary and impurity phases. The XRD pattern for prepared Bi_2WO_6 (BW) is provided as the electronic supplementary information (ESI) in Fig. S1.

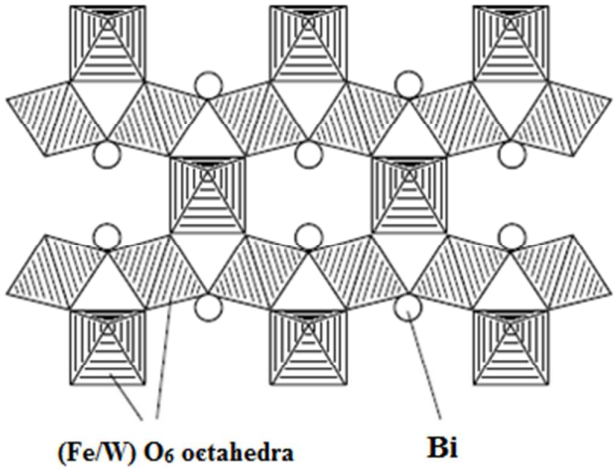

Figure. 4 Schematic representation of the crystal structure of BiFeWO6

Fig. 4 shows the structure of β-pyrochlore structured $BiFeWO_6$.[27] It can be envisaged that the structure of $BiFeWO_6$ is built up of corner sharing $(Fe/W)O_6$ octahedra creating networks of hexagonal channels along c-axis and Bi ions are located in these channels. It should also be noted that the bismuth oxides containing d^n cations adopt centrosymmetric structures, where the metal-oxygen octahedral are periodically arranged and thereby they adopt a defect pyrochlore structure.[28]

Morphological Analysis

Morphology analysis using FESEM (Hitachi SU6600, Singapore) technique revealed the spherical morphology of the synthesized $BiFeWO_6$ nanoparticles (Fig 5(a)-(c)).

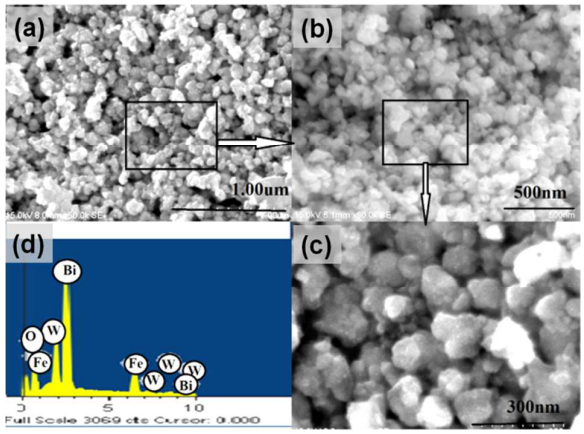

Figure. 5 (a-d) FESEM micrographs and EDS spectrum of $BiFeWO_6$

It is evident from the images that the nanoparticles are homogenously distributed with relatively reduced agglomeration. The formation of spherical morphology is possible in the co-precipitation method as it takes place in the acidic medium. It can be observed in the synthesis process that the digestion of acidic solution with a base and formation of precipitation are likely a simultaneous process. Under such circumstances, the acidic nature of the solution controls the particle agglomeration and leads to the thermodynamically stable shape, which is the spherical. Figure 5(d) shows the energy dispersive spectrum that qualitatively confirms the existence of Bi, Fe, W and O elements in the sample and no trace of any other elements.

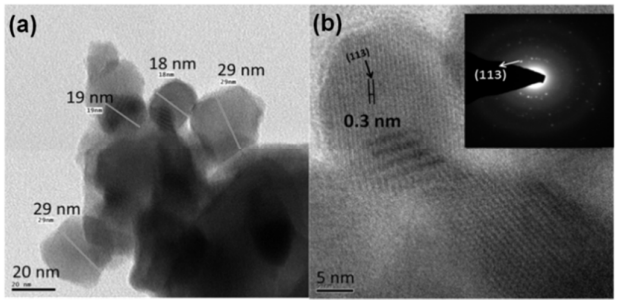

Figure 6 (a) HRTEM images and (b) SAED pattern of $BiFeWO_6$ NPs

The HRTEM (Tecnai T30 G2 S-Twin, FEI company) micrograph obtained is shown in Fig. 6(a). The micrograph obtained is also in good agreement with the FESEM micrographs in terms of the particle morphology and aggregation nature. The size of the particles is measured from the micrographs and the average particle size is found to be 24 nm. Fig. 6(b) and its inset image show the lattice fringes and selected area electron diffraction (SAED) pattern of the BFWO NPs, respectively. The measured lattice distance (d) in the fringes image and distance of the circular pattern in SAED image is found to be 0.3 nm which is corresponding to the inter-planar distance of (113) plane. This measured value is also in agreement with the value given in standard JCPDS #38-1285.

Optical and Band gap Analysis

The UV-Vis diffuse reflectance profile of BFWO NPs and BWO are shown in Fig. 7. It can be seen that absorption edge for Bi_2WO_6 is found to be around 400 nm, where as for $BiFeWO_6$ the absorption edge is around 500 nm. The observed red shift may be attributed to the Fe modification on the structure of bismuth tungstate. The inset graph of Fig. 7 shows the Kubelka Munk (KM) plot of BFWO NPs and BWO, drawn the photon energy as the function of KM intensity. The band gap energy of the BFWO NPs and BW is estimated from the extrapolated KM plot and is found to be 2.35 eV and 3.1 eV respectively. The band gap of BFWO NPs is relatively lower than that of BWO, which is of benefit to its visible light driven photocatalytic efficiency. Further, the observed steep edge in the lower wavelengths could be attributed to the intrinsic transitions that occurred as an implication of the impurity free nature of the synthesized BFWO NPs.[29]

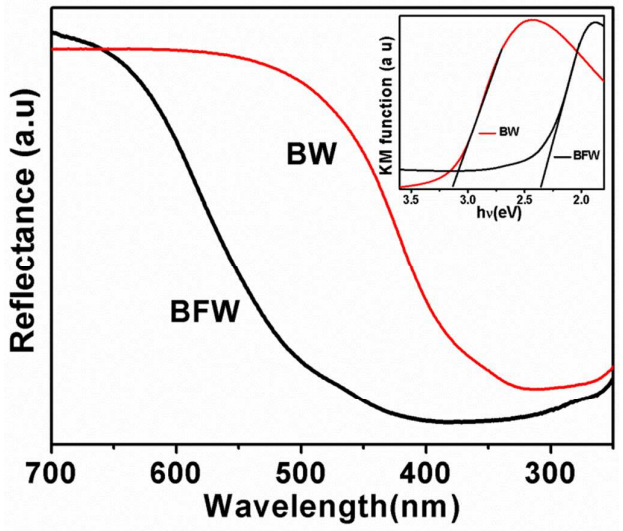

Figure. 7 UV-DRS profile and Kubelka Munk plot illustrating the band gap energy of $BiFeWO_6$ and Bi_2WO_6

It should be noted that the formation of band structure in BFWO NPs is essentially due to the hybridization of the *s* and *d* states of Bi, Fe, and W with O 2p states. Such hybridization also leads to an up-shift of the valence band maximum (VBM) in the band structure and offers a control over the band edge positions in the BFWO NPs.[30]

For the photocatalytic activity, the band gap edge positions of a photocatalyst play crucial roles as their energy levels should be appropriate for the process of photo-excitation and dissociation of the excited carriers to the surrounding medium. Accordingly, the band edge positions (VBM and CBM) of the synthesized BWFO NPs are estimated from the following empirical formula .[31]

$$E_{CB} = X - 0.5E_g - E_0$$

$$E_{VB} = E_{CB} - E_g$$

where E_g is the band gap energy determined from UV-DRS spectrum, E_0 is the factor relating the reference electrode redox level to the absolute vacuum scale ($E_0 = 4.5\ eV$ for normal hydrogen electrode), and X is the electronegativity of the semiconductor, which can be expressed as the geometric mean of the absolute electronegativity of the constituent atoms. Electronegativity of $BiFeWO_6$ is estimated to be 6.1 eV, given the equation above E_{CB} is calculated to be 0.4 eV. Based on the above calculations, a comparative picture of WO_3, Bi_2WO_6 and $BiFeWO_6$ with their band gap energy and relevant band edge positions are given in Fig.8.

It can be proposed from Fig. 8 that tungstate based materials are potential for water splitting provided their CBM is positioned with that of the hydrogen potential. Experimentally it is proven that WO_3, upon inclusion of Bi_2O_3 transforms to Bi_2WO_6 with band gap of 2.8 eV which has been effectively used for water splitting application.[32] From this we understand

that the layered perovskite structure of Bi_2WO_6 favours CBM shifting but has not reduced band gap energy. This is also found to be inconsistent with the band gap values obtained using UV – DRS, where BFWO NPs has a band gap of 2.35 eV and BWO with 3.1 eV.

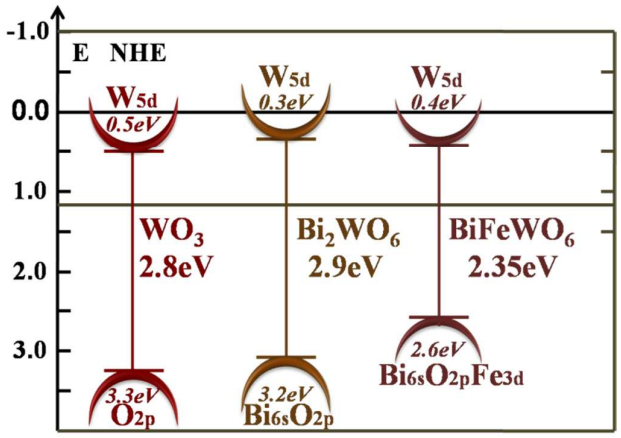

Figure. 8 Comparison of band edge offset and band gap energy values of WO3, Bi2WO6 and BiFeWO6

On the other hand, theoretically WO_3 has a CBM of 0.7 eV, whereas, Bi_2WO_6 has CBM of 0.3 eV which are empirically calculated from the above equation. In a similar way, $BiFeWO_6$ has CBM of 0.4 eV but reduced band gap energy of 2.35 eV i.e inclusion of d^n transition and Bi elements in tungstate show pyrochlore structure where the CBM upward shift is also accompanied with reduction in band gap energy. It is understood that the synthesised BFWO Nps exhibiting CBM upward shift and reduced band gap energy are due its pyrochlore structure Therefore, making use of the flexibility of pyrochlore, the band gap engineering can be done by introducing the high electronegative transition elements, which makes the material more potential for photocatalytic water splitting applications.

Photocatalytic Activity

Photocatalytic Degradation of Methylene blue

Fig. 9(a)-(b) show the degradation spectra of MB dye and the degradation efficiency (C/C_0) graph, respectively. It can be noted from fig 9-(b) that the BFWO NPs took an average time of 4 h to degrade the given amount of dye while commercial TiO_2 degrades only 20% and Bi_2WO_6 degrades 40% under identical conditions. Also from the full range 200 – 800nm UV-Vis absorption spectra it is understood that MB dye degrades in the presence of BFWO NPs without any intermediate.[33-34] The mineralisation of MB dye during the course of photodegradation using BFWO NPs is shown in ESI Fig. S2. From Fig. 9(b), it is clear that the photocatalytic efficiency of BFWO is higher than that of BWO. The observed increased photocatalytic efficiency of BFWO could be attributed to the incorporation of Fe into the lattice of BWO system. It is known that the Fe atoms are optical active and their (Fe 3d) hybridization with oxygen (O 2p) atoms caused a shift in the band edge positions in BWO nanoparticles. In this context, we claim that the Fe atoms in BWO lattices significantly modified their electronic and optical properties through hybridization process that synergistically enhanced their photocatalytic efficiency as well. The Langmuir-Hinshelwood model was applied to quantitatively understand the reaction kinetics of the photo-degradation of the MB. According to the model, the first order rate constant k is calculated by $(C_0 - C_t)/t$, where C_0 is the initial concentration of the dye and C_t is the concentration of the dye at the end of t time, which was taken as 180 min. The value of k is found to be 0.0011 min-1. A similar k value was also reported for potassium chromium tungstate.[35] The photocatalytic degradation of phenol using BFWO NPs is shown in ESI Fig. S3.

OH radical detection

In aqueous solution, the photocatalytic degradation of pollutants is caused by active OH species produced on the surface of the metal oxide semiconductors. The degradation rate is directly proportional to the probability of formation of the hydroxyl radicals on the catalyst surface. The detection of Oh radicals by BFWO NPs under visible light irradiation was carried using Terephthalic acid as probe.

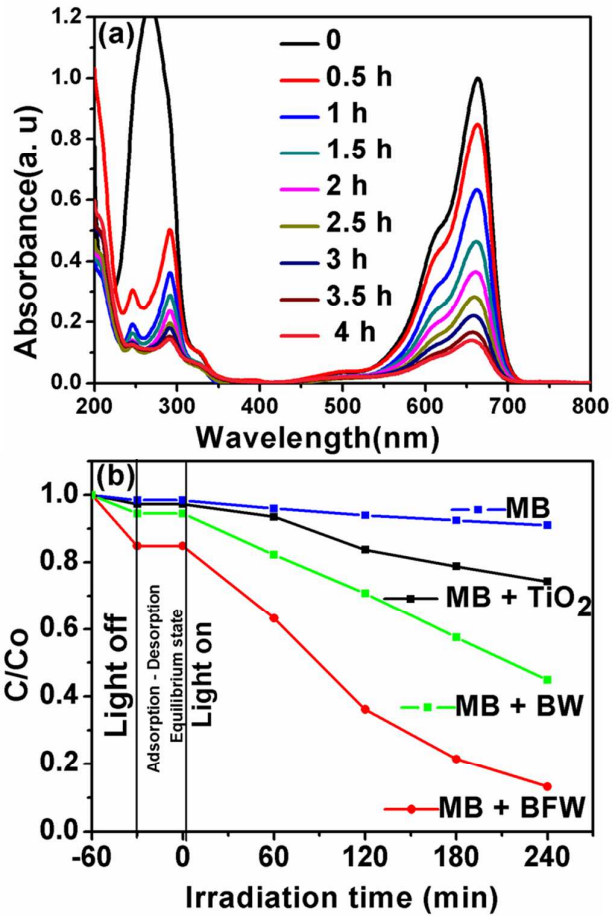

Figure 9. (a-b) Degradation spectra of methylene blue using $BiFeWO_6$ and degradation efficiency of the prepared nano-photocatalyst $BiFeWO_6$, Bi_2WO_6, and TiO_2.

The spectrum recorded using fluorescence property of 2 hydroxy terephthalate, which results due the interaction of OH radical of BFWO NPs and terephthalic acid under visible light irradiation is shown in Fig 10. The PL intensity steadily increases after light irradiation, indicating the formation of active OH species by the BFWO NPs. Based on the Luan et al., the photocatalytic degradation mechanism of MB under visible light irradiation can be proposed as follows (Luan et al. 2009):[36]

$$SC(\mathrm{BFWONp}) + hv \rightarrow SC(\mathrm{BFWONp})(h^{+}_{\mathrm{VB}} + e^{-}_{\mathrm{CB}})$$

$$O_2 + e^{-}_{\mathrm{CB}} \rightarrow \dot{O}^{-}_{2}$$

$$H_2O + h^{+}_{\mathrm{VB}} \rightarrow \dot{O}H + H^{+}$$

Or

$$MB + h^{+}_{\mathrm{VB}} \rightarrow M\dot{B}^{+} \rightarrow products$$

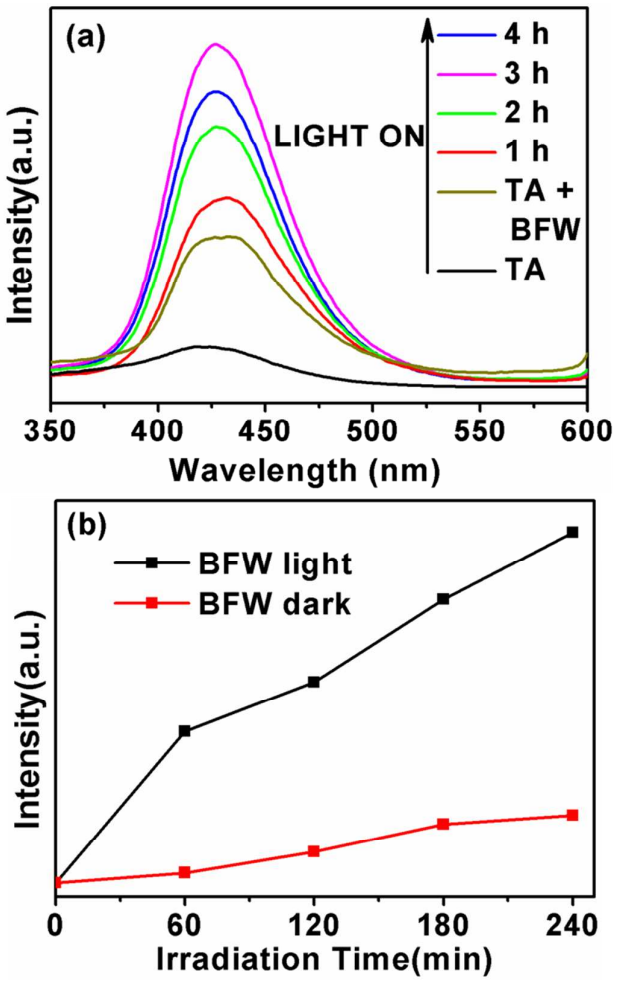

Figure 10. (a) OH-trapping PL spectra of BiFeWO6 in solution of TA at room temperature (ex, 312 nm; em, 426 nm) and (b) plot of the induced fluorescence intensity at 426 nm against irradiation time under visible light for BiFeWO6 under light and dark..

Electrochemical Impedance spectroscopy

EIS measurement was also used to investigate the charge transfer resistance and the separation efficiency between the photogenerated electrons and holes. Fig. 11 shows EIS Nyquist plots of BFW NPs under dark and light irradiated conditions. It can be seen that the arc radius on EIS Nyquist plot of BFW NPs under light irradiation is smaller than that of BFW NPs in dark. This indicates a fast interfacial charge transfer process and effective separation of photogenerated electron-hole pairs. This enhanced separation efficiency and interfacial charge transfer efficiency of photogenerated electron-hole pair contribute to the photocatalytic activity of the BFW NPs.

Stability

It is well known that practical application of a photocatalyst are dependent on its stability, to ensure the stability BFWO NPs were characterised for XRD and is shown in Fig. 11 .It is inferred that BFWO NPs are highly stable after photocatalytic process. The repeatability test for BFWO NPs was performed and the results are shown in ESI Fig S4, where the photocatalytic efficiency of the photocatalyst is found to be consistent in all five cycles.

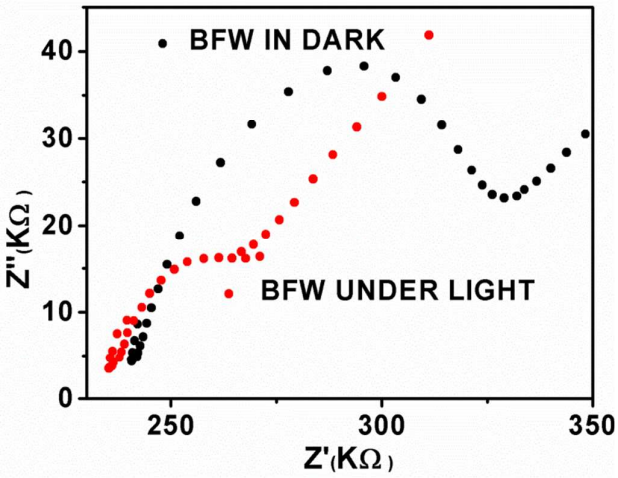

Figure. 10. Electrochemical impedance spectra of BiFeWO6 under dark and light irradiation.

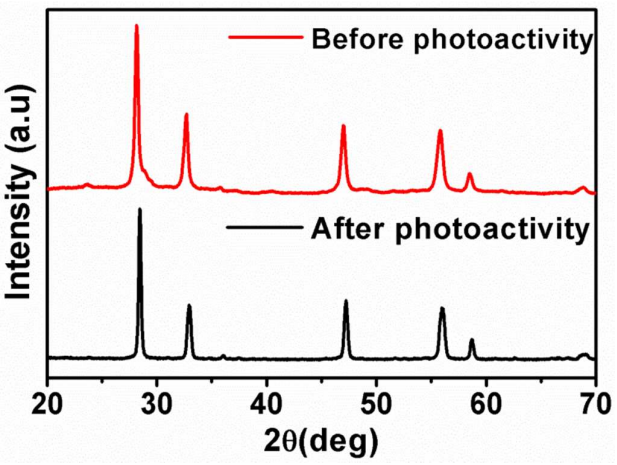

Figure. 11XRD Pattern BiFeWO6 before and after photocatalytic activity.

Photocatalytic efficiency of BFWO NPs

The observed photocatalytic efficiency in BFWO NPs can be accounted to the reduced band gap energy (2.35 eV) and smaller particle size (15 nm – 30 nm). Further to this, the reduced band gap energy could be demonstrated according to the crystal field theory. In a system of tungstate, such as BFWO, the crystal field around WO_6 octahedra is the key factor for the band gap energy and its band edge positions.[37] In such WO_6 octahedra system, the shorter W-O bond length leads to increased crystal field strength in the material and hence increase in splitting of energy levels. It was reported in the crystal structure of tungstates the average W-O distance in WO_3 is 1.91 Å,[38] whereas, in defect pyrochlore it is 1.95 Å.[28] It is noteworthy that shorter bond length has stronger crystal field leading to higher splitting of W 5*d* orbital and hence increase in band gap energy. The increase in W-O bond length of defect pyrochlore has reduced crystal field, less splitting of W 5*d* orbital and reduced bandgap energy value. Therefore, in the BFWO system, the observed photocatalytic behaviour could be assigned to the increase in W-O bond length due to the localisation of Bi^{3+} and Fe^{3+} ions in the lattices of this defect pyrochlore structured BFWO NPs. Further, the Bi^{3+} and Fe^{3+} ions have also caused the dispersion of 6*s* and 3*d* orbital in the valence band and resulting in upward shift of VBM. Similarly, the hybridisation of Bi 6*s* and Fe 3*d* also reduces the splitting if W 5*d* orbital and resulting in an upward shift of CB_{max}.[39] Nevertheless, such perspective should yet to be explored in this field that may increase the scope of tungstate based materials to be employed as potential materials for both visible light induced photocatalytic degradation and water splitting applications.

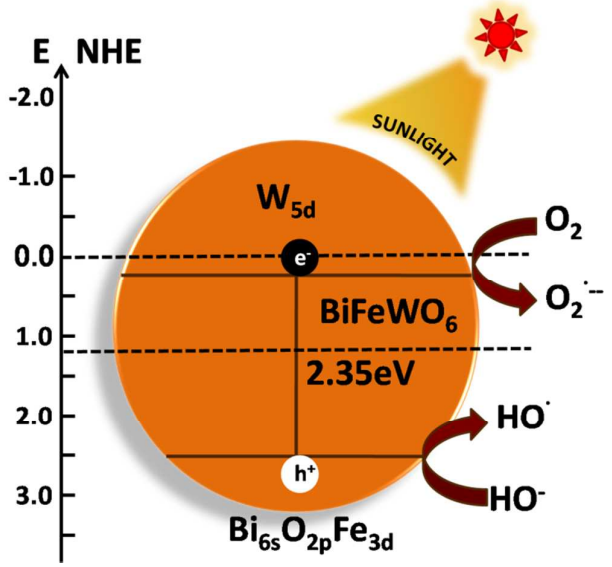

Figure 12.Schematic representation of sunlight driven BiFeWO6

It is also to be noted that the smaller particle size of the synthesized BFWO NPs favour photocatalytic process through the fast migration of excited electrons and holes to surface causing a delay in their recombination process. This essentially leads to increased number of active sites on the surface of the photocatalyst. The conception of the observed photocatalytic efficiency that is associated with the particle size of the BFWO NPs and band gap is depicted in Fig. 12.

Conclusion

In conclusion, novel photocatalytic $BiFeWO_6$ nanoparticles have been synthesized via co-precipitation method. Its structure has been determined using, XRD and the lattice parameters are found to be a = 5.582 Å, b = 5.524 Å, c = 16.064 Å. The particle sizes were in the range of 15nm - 30 nm and it has a band gap of 2.35 eV. It shows visible light photocatalytic degradation of methylene blue under solar radiation of 1,20, 000 lux. This study gives a strategy of engineering the band of tungstate with regard to establishment of the band offset and band gap reduction to synthesize single phased metal oxides. Further work on this material to tune its electronic structure by making use of the flexibitlity of pyrochlore extends its application to photolyse as well as to photoremediate contaminated water simultaneously. Such concept would eventually lead to the identification of single phase oxide as efficient visible light driven photocatalyst.

Acknowledgements

Authors gratefully acknowledge the support of the NCNSNT research grant and DST – PURSE programme, University of Madras to carry out this research work

References

1 Gur. N. A, Fromer. M. L, Geier and A. P. Alivisatos, *Science*, 2005, **310**, 462.
2 A. Fujishima and K. Honda, *Nature,* 1972, **238**, 37.
3 Z. G. Zou, J. H. Ye, K. Sayama and H. Arakawa, *Nature*, 2001, **414**, 625.
4 De. G. C, Roy. A. M, Bhattacharya .S. S, *Int. J. Hydrogen Energy,* 1996, **21**, 19.
5 Hwang. D. W, Kim. J, Park. T. J, Lee. J. S, *Catal. Lett.,* 2002, **80**, 53.
6 R. A. Rakkesh and S. Balakumar, *Process and Appl. of Ceramics,* 2014, **8**, 7.
7 M. Sakar, S. Balakumar and S. Ganesamoorthy, *J. Mater. Chem. C*, 2014, **2**, 6835.
8 R. Ajay Rakkesh, D. Durgalakshmi S. Balakumar, *J. Mater. Chem. C*, 2014,**2**, 6827.
9 A. Kudo, Y. Miseki, *Chem. Soc. Rev.*, 2009, **38**, 253.
10 Zeng. J; Wang. H, Zhang. Y. C, Zhu. M. K, Yan. H, *J. Phys. Chem. C,* 2007, **111 (32)**, 11879.
11 Subramanian .M. A, Aravamudan. G, Rao. G. V. S, *Prog. Solid State Chem.,* 1983, **15 (2)**, 55.
12 Tuller. H. L., *Solid State Ionics,* 1992, **52**, 135.
13 Vandijk.M. P., Burggraaf.A. J., Cormack.A. N., Catlow.C. R. A., *Solid State Ionics,* 1985, **17 (2)**, 159..
14 M. Sakar and S. Balakumar, *RSC Adv.*, 2013, **3**, 23737.
15 S. Murugesan, M. N. Huda, Y. Yan, M. M. Al-Jassim and V. Subramanian, *J. Phys. Chem. C,* 2010, **114**, 10598.

16 H. Fu, C. Pan, W. Yao and Y. Zhu, *J. Phys. Chem. B*, 2005, **109**, 22432.
17 J. Yu and A. Kudo, *Adv. Funct. Mater.,* 2006, **16**, 2163.
18 Z. Zou, J. Ye and H. Arakawa, *J. Mater. Res*., 2001, **16**, 35.
19 Kudo. A and Hijii. S, *Chem. Lett.,* 1999, **8**, 1103.
20 M. Valant, G. S. Babu, M. Vrcon, T. Kolodiazhnyi and A. K. Axelsson, *J. Am. Ceram. Soc*., 2012, **95**, 644.
21 A. Kudo and Y. Miseki, *Chem. Soc. Rev*. 2009, **38**, 253.
22 R. Abe, H. Takami, N. Murakami and B. Ohtani, *J. Am. Chem. Soc.*, 2008, **130,** 7780.
23 C. Janaky, K. Rajeshwar, N. R. De Tacconi, W. Chanmanee and M. N. Huda, *Catal. Today*, 2013, **199**, 53.
24 N. Zhang, R. Ciriminna, M. Pagliaro and Y.-J. Xu, *Chem. Soc. Rev.*, 2014, **43**, 5276.
25 A. Ramanan, G. N. Subbanna, J. Gopalakrishnan, and C. N. R. Rao, *Rev. Chim. Miner*., 1983, **20**, 576.
26 J. Rout, B.N. Parida, P. R. Das ,R. N. P. Choudhary, *J. of Elect. Mat*., 2013, **3**, 732.
27 S. Ikeda, T. Itani, K. Nango and M. Matsumura, *Catalysis Letters*, 2004, **98**, 229.
28 A. Ramanan, J. Gopalakrishnan, C. N. R. Rao, *Journal Of Solid State Chemistry,* 1985, **60**, 376.
29 Kudo .A, Tsuji .I, Kato .H, *Chem. Commun.,* **2002**, 1958.
30 H. Tong, S. Ouyang, Y. Bi, N. Umezawa, M. Oshikiri and Jinhua .Y, *Adv.Mater*., 2012, **24**, 229.
31 Lv. J, Kako. T, Zou. Z. G, Ye. J. H, *Appl. Phys. Lett*. 2009, **95**, 032107.
32 Charlene. N, Akihide. I, Yun. H. N, and Rose .A, *J.Phys.Chem.Lett*., 2012, **3**, 913.
33 T. Zhang, T. Oyama, A. Aoshima, H. Hidaka, J. Zhao, N. Serpone, *J. PhotoChem.PhotoPhys,* 2001, **A 140,** 163–172.
34 Soo-Keun Lee and Andrew Mills ,*Chem. Commun*., 2003, **18**, 2366–2367.
35 G. Ravi , N. K.Veldurthi, M. D. Prasad, N. R. Muniratnam, G. Prasad, M. Vithal, *J Nanopart Res,* 2013, **15**:1939.
36 Luan J, Zhao W, Feng J, Cai H, Zheng Z, Pan B, Wu X, Zou Z, Li Y, *J Hazard Mat*, 2009, **164**, 781.
37 M. Oshikiri, M. Boero, J. Ye, Z. Zou and G. Kido, *J. Chem. Phys.*, 2002, **15**, 7313.
38 E. Salje, *Acta Crystallogr., Sect. B*, 1977, **33**, 574.
39 Junwang .T and Jinhua .Y, *J. Mater. Chem*., 2005, **15**, 4246.